

Split-Cylinder Resonant Electron Polarimeter

R. Talman, LEPP, Cornell University;
B. Roberts, University of New Mexico;
J. Grames, A. Hofler, R. Kazimi, M. Poelker, R. Suleiman;
Thomas Jefferson National Laboratory

September 24, 2017

Abstract

Passive (non-destructive) high analysing power polarimetry will be required for feedback stabilization of frozen-spin storage rings. This is especially true for electrons. This paper proposes such an electron polarimeter. A basic resonator cell (similar to those commonly used for NMR detection) is a several centimeter long copper split-cylinder, with gap serving as the capacitance C of, for example, a 1.75 GHz LC oscillator, with inductance L provided by the conducting cylinder acting as a single turn solenoid. Eight such cells, regularly arrayed along the beam, form a meter-long polarimeter. The magnetization of a longitudinally-polarized electron bunch passing through the resonators coherently excites their fundamental oscillation mode and the coherently-summed response from all resonators measures the polarization. “Background” due to direct charge excitation is suppressed by arranging successive beam bunches to have alternating polarizations. This moves the beam polarization frequency away from the direct beam charge frequency. Along with charge-insensitive resonator design, modulation-induced sideband excitation, and synchronous detection, the magnetization “foreground” is isolated from the background. Such extreme background rejection measures are made necessary by the large value of electron charge relative to electron magnetic dipole moment. The same measures that suppress background can be exploited to suppress spurious signals due to apparatus misalignment. A test of the polarimeter is proposed using a polarized, 0.5 MeV kinetic energy, 0.5 GHz bunch frequency linac electron beam at the Jefferson Laboratory.

Contents

1	Introduction	3
2	Polarimeter design	4
2.1	Apparatus	4
2.2	Resonator parameters	7
3	“Local” Lenz law (LLL) approximation	8
4	Foreground magnetization excitation calculation	11
5	Background resonator excitation by bunch charge	13
5.1	Off-axis, parallel particle incidence	15
5.2	Canted particle incidence	16
6	Synchronous signal processing	18
6.1	Coherent summation of resonator outputs	18
6.2	Why synchronous detection? Why helicity matters?	21
	Digression:	22
7	Modulation-induced, foreground/background separation	22
8	Circuit analysis	23
9	Frequency choice considerations	24
10	Misalignment compensation budget	25
11	Recapitulation and conclusions	28

1 Introduction

A proposed experiment to measure the electron electric dipole moment (EDM) uses polarized electrons in a storage ring in which both bending and focusing is produced by purely electric elements. The beam polarization will be “frozen”, parallel or anti-parallel to the beam direction. Polarimetry is required to monitor and stabilize this frozen spin operation. Acting on whatever EDM the electron possess, the radial electric bending field tends to tip the beam polarizations up or down. It is this tipping that is to be measured to obtain the electron EDM. Ability to perform this measurement sets stringent requirements on the polarimetry—the measurement has to be non-destructive and have high analysing power. This is the motivation for the present paper.

This paper is concerned only with measuring the polarization of an electron beam by measuring the bunch magnetization resulting from the electron’s magnetic dipole moment (MDM). An apparatus capable of this polarimetry is proposed, and a test of its polarimetry performance using a longitudinally polarized 0.5 MeV kinetic energy, 500 MHz bunch frequency linac electron beam at Jefferson Laboratory is described.

The fundamental impediment to resonant electron polarimetry comes from the smallness of the magnetic moment divided by charge ratio of fundamental constants,

$$\frac{\mu_B/c}{e} = 1.930796 \times 10^{-13} \text{ m}, \quad (1)$$

where, except for a tiny anomalous magnetic moment correction and sign, the electron magnetic moment is equal to the Bohr magneton μ_B . This ratio has the dimension of length because the Stern-Gerlach force due to magnetic field acting on μ_B , is proportional to the *gradient* of the magnetic field. To the extent that it is “natural” for the magnitudes of E and cB to be comparable, Stern-Gerlach forces are weaker than electromagnetic forces by ratio (1). This adverse ratio needs to be overcome in order for magnetization excitation to exceed direct charge excitation. Methods to do this include charge-insensitive resonator design, shifting magnetization frequency relative to charge frequency, and utilizing differential modulation to distinguish between charge and magnetization. “On paper” these measures will be enough to distinguish foreground from background. But to be fully persuasive, this will have to be confirmed by experiment.

Potentially as serious an impediment to resonant polarimetry is the smallness of the ratio of magnetization energy U^{pol} . (given by Eq. (13)) relative to thermal energy $k_B K$, where k_B is Boltzmann’s constant and K is absolute temperature. (Unlike the adverse magnetization/charge ratio) this adverse thermal ratio is ameliorated by the squared number of electrons per bunch, N_e^2 , by a resonant enhancement ratio, $M_r^2 \approx 10^6$, by the squared number of resonating cells N_{cell}^2 , and by the resonator frequency f_c (which multiplies the resonant cavity energy by the number of cycles per second to produce the measurable signal power). As the bottom line of Table 2 shows, this proportionality to f_c favors high frequency. There is also a minor multi-resonator penalty, in that the r.m.s. thermal resonator energy has been increased by a factor $\sqrt{N_{\text{cell}}}$.

The adverse thermal energy ratio could be ameliorated by running the resonator at cryogenic temperature. But, for present purposes, this paper refrains from exploiting this possibility. (One of the intended eventual applications will use resonant polarimetry to stabilize frozen spin proton storage ring polarization control. The fact that the proton’s MDM is three orders of magnitude smaller than the electron’s all but demands cryogenic operation for resonant proton polarimetry. Fortunately, though, because of their greater stiffness, the number of frozen spin particles per bunch N_p can be much greater for protons than for electrons.)

With the electron beam bunching assumed to be perfectly periodic, the magnetization signal can, at least in principle, emerge from the thermal noise floor by synchronous detection over sufficiently long runs. According to the bandwidth-duration principle, the effective band width of a mono-frequency input depends inversely on the run duration. As a result the total noise energy (obtained by time-integrating the noise power) is independent of run duration. By contrast, since the magnetization power is constant over time, its time-integrated value will eventually exceed the noise energy, causing

the magnetization signal to emerge from the thermal noise floor. This is quantified by the bottom two rows of Table 2. One sees from these entries, though, that the expected magnetization signal is very weak and challenging to detect. The detection time for accurate measurement of beam polarization is likely to be measured in minutes.

2 Polarimeter design

2.1 Apparatus

The proposed resonator design, shown in Figure 1, was introduced by Hardy and Whitehead[1] for NMR measurements, and has been used commonly for this purpose in low temperature experiments such as reference [2].

Consider a single, longitudinally polarized bunch of electrons in a linac beam that passes through the split-cylinder resonator. The split cylinder can be regarded as a one turn solenoid. For reasons explained later, the bunch polarizations will toggle, bunch-to-bunch, between directly forward and directly backward. This is achieved by having two oppositely polarized, but otherwise identical interleaved beams, an A beam and a B beam, each having bunch repetition frequency $f_0 = 0.25$ GHz (4 ns bunch separation). The resonator harmonic number relative to f_0 is an odd number in the range from 1 to 11; this immunizes the resonator from direct charge excitation. Irrespective of polarization, the A+B-combined bunch-charge frequencies will consist only of harmonics of $2f_0 = 0.5$ GHz, incapable of exciting the resonator(s).

In practice the bunches will be somewhat less than fully polarized but, for estimating the signal strength and foreground to background ratio, we assume the bunches are 100% longitudinally polarized.

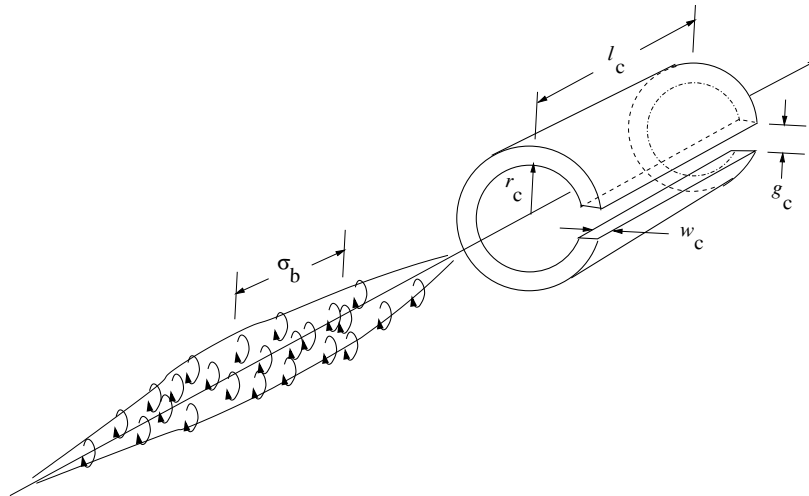


Figure 1: Perspective view of polarized beam bunch passing through the polarimeter. Dimensions are shown for the polarized proton bunch and the split-cylinder copper resonator, and listed in Table 1. More refined design parameters for such a resonator are given in a paper by Hardy and Whitehead[1]. They also provide formulas for the changes in resonator parameters when the overall apparatus is shielded from the outside world by a cylindrical conductor of radius r_S —which could, for example, be $r_S = 4r_c$, depending on the resonator wall thickness w_c . For the proposed test, using a polarized electron beam at Jefferson Lab, the bunch will actually be substantially shorter than the cylinder length, and have a beer can shape.

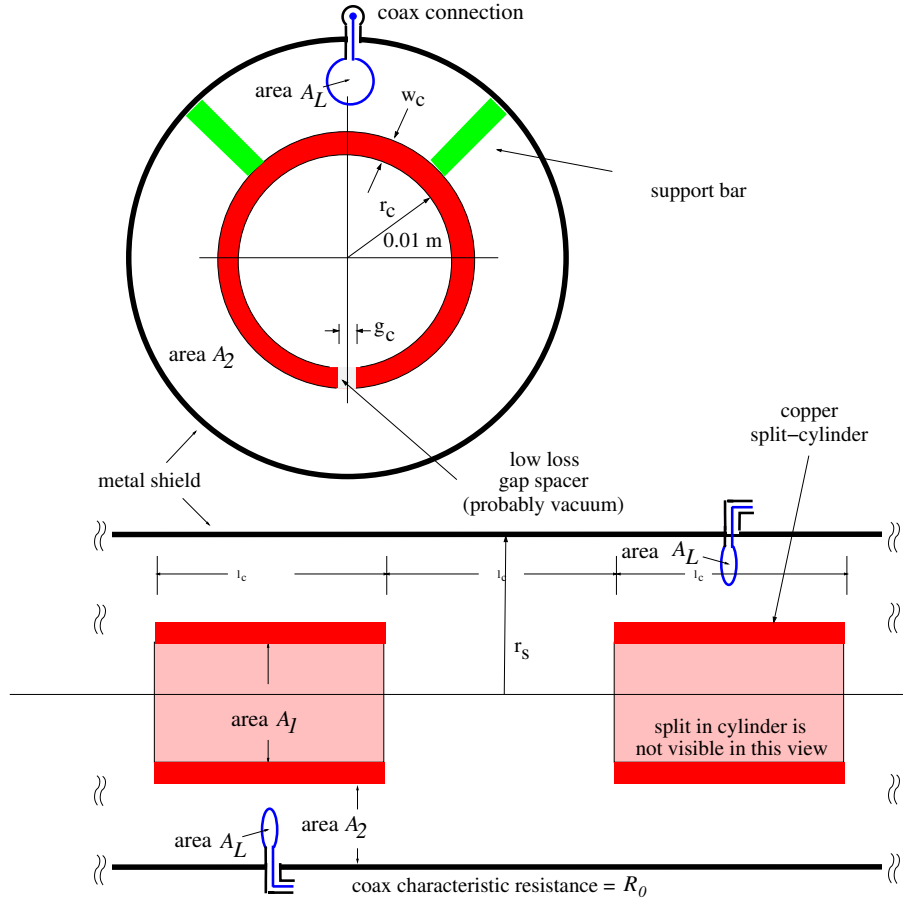
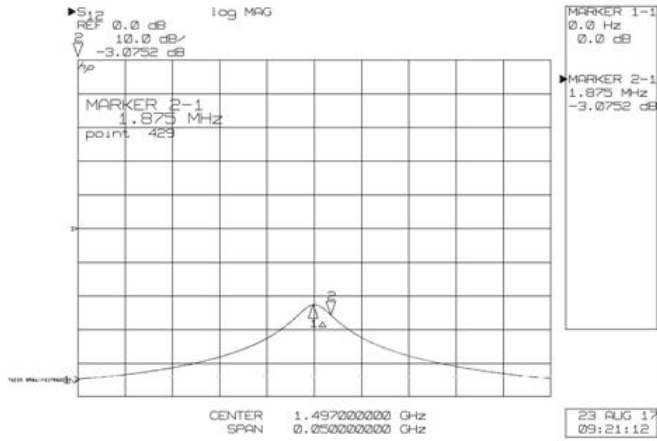


Figure 2: End view (above) and side view (below) of two resonant split-cylinder polarimeter cells. The cell resonant frequencies are matched to both the electron bunch passage frequency and the transit time through individual split-cylinders. Signals from individual resonators are loop-coupled out to coaxial cables with characteristic resistance R_0 . With unloaded quality factor Q_{un} , the effective resistance of the inductance L_c is $r = \omega_c L_c / Q_{un}$, and the optimal coupling factor is of order 1 percent. The natural frequency is inversely proportional to $r_c^2 w_c / g_c$, which makes it strongly temperature dependent. By supporting the split cylinder by material less expansive than the outer conductor, the gap spacing can have exaggerated denominator temperature expansion, compensating for the numerator temperature dependence. Perhaps the frequency trimming can be incorporated through the same elements, similarly exploiting the extreme mechanical weakness of the split cylinder?



Outer cylinder ID: 2.36", OD: 2.64, Length: 2.8"

Inner split ring resonator ID: .85" OD .98", split width .062", length: 2.13"

Figure 3: The upper figure is a photograph of prototype split-ring resonators that has been built at the University of New Mexico. The lower figure shows the spectral response of the resonator, showing a resonance at 1.472 GHz, close to the design frequency. The unloaded Q-value is 800, much reduced by radiation out the ends.

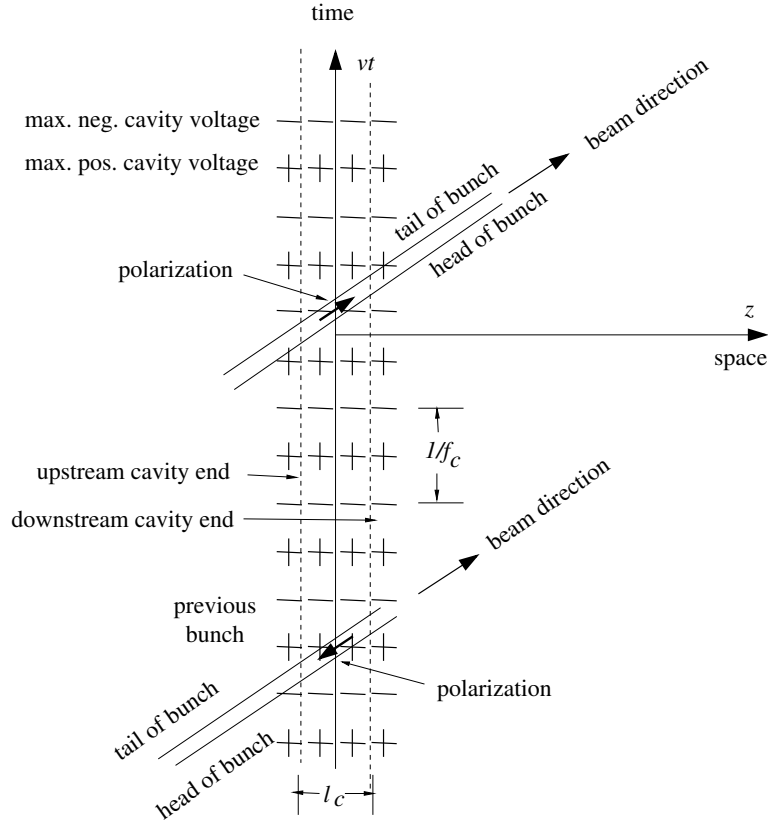


Figure 4: Space-time plot showing entry by the front, followed by exit from the back of one bunch, followed by the entrance and exit of the following bunch. Bunch separations and cavity length are arranged so that cavity excitations from all four beam magnetization excitations are perfectly constructive. The rows ++++ and ---- represent equal time contours of maximum or minimum V_C , E_ϕ , dB_z/dt , or dI_C/dt , all of which are in phase. (Unlike all other figures and examples, which use $h_c = 11$) for this figure (to save space) the harmonic number is $h_c = 7$.

2.2 Resonator parameters

Treated as an LC circuit, the split cylinder inductance is L_c and the gap capacity is C_c . The highly conductive split-cylinder can be treated as a one-turn solenoid. (For simplicity, minor corrections due to the return flux are not included in formulas given here, but are included later.) In terms of its current I , the magnetic field B is given by

$$B = \mu_0 \frac{I}{l_c}, \quad (2)$$

and the magnetic energy W_m can be expressed either in terms of B or I ;

$$W_m = \frac{1}{2} \frac{B^2}{\mu_0} \pi r_c^2 l_c = \frac{1}{2} L_c I^2. \quad (3)$$

The self-inductance is therefore

$$L_c = \mu_0 \frac{\pi r_c^2}{l_c}. \quad (4)$$

The gap capacitance (with gap g_c reckoned for vacuum dielectric and fringing neglected) is

$$C_c = \epsilon_0 \frac{w_c l_c}{g_c}. \quad (5)$$

Because the numerical value of C_c will be small, this formula is especially unreliable as regards its separate dependence on w_c and g_c . Furthermore, for low frequencies the gap would contain dielectric other than vacuum. Other resonator parameters, with proposed values, are given in Table 1 and, in greater generality, in Table 2.

parameter name	parameter symbol	formula	unit	value
cylinder length	l_c		m	0.04733
cylinder radius	r_c		m	0.01
gap height	g_c		m	0.00103943
wall thickness	w_c		m	0.002
capacitance	C_c	$\epsilon_0 \frac{w_c l_c}{g_c / \epsilon_r}$	pF	0.47896
inductance	L_c	$\mu_0 \frac{\pi r_c^2}{l_c}$	nH	7.021 3
resonant freq.	f_c	$1/(2\pi\sqrt{L_c C_c})$	GHz	2.7445
resonator wavelength	λ_c	c/f_c	m	0.10923
copper resistivity	ρ_{Cu}		ohm-m	1.68e-8
skin depth	δ_s	$\sqrt{\rho_{Cu}/(\pi f_c \mu_0)}$	μm	1.2452
eff. resist.	R_c	$2\pi r_c \rho_{Cu}/(\delta_s l_c)$	ohm	0.017911
unloaded. qual. factor	Q			6760.0
effective qual. fact.	Q/h_c			643.65
bunch frequency	$f_A = f_B = f_0$		GHz	0.2495
cavity harm. number	h_c			11
electron velocity	v_e	$c\sqrt{1-(1/2)^2}$	m/s	2.5963e8
cavity transit time	Δt	l_c/v_e	ns	0.18230
transit cycle advance	$\Delta\phi_c$	$f_c \Delta t$		0.50032
entry cycle advance		$\Delta\phi_c l_b/l_c$		0.15011
electrons per bunch	N_e			2.0013×10^6
bunch length	l_b		m	0.0142
bunch radius	r_b		m	0.002

Table 1: Resonator and beam parameters. The capacity has been calculated using the parallel plate formula. The true capacity will probably be somewhat greater, and the the gap g_c will have to be adjusted to tune the natural frequency. When the A and B beam bunches are symmetrically interleaved, the bunch repetition frequency (with polarization ignored) is $2f_0$.

3 “Local” Lenz law (LLL) approximation

A “local” Lenz law approximation for calculating the current induced in our split cylinder by a passing polarized beam bunch is illustrated by Figure 5. The split cylinder resonator is treated as a one turn solenoid and, for simplicity, the electron bunch is assumed to have a beer can shape, with length l_b and radius r_b . (For the proposed Jefferson Lab test this approximation is actually excellent.) The magnetization \mathbf{M} within length Δz of a beam bunch (due to all electron spins in the bunch pointing, say, forward) is ascribed to azimuthal Ampèrian current $\Delta I_b = i_b \Delta z$. In other words, in the volume within the beam bunch the magnetic field is also a perfect solenoid (with end fields being neglected).

For sufficiently short cylinder lengths, the bunch transit time will be shorter than the oscillation period of the split cylinder and the presence of the gap in the cylinder produces little suppression of the Lenz's law current induced by the passing bunch (because the capacitance of the gap has not had time to charge up). Define i_{LL} to be the Lenz law current per longitudinal length. Then $\Delta I_{LL} = i_{LL}\Delta z$ is the induced azimuthal current shown in the (inner skin depth) of the cylinder, in the "local region" of the figure. To prevent any net flux from being present locally within the section of length Δz , the flux due to the induced Lenz law current must cancel the Ampère flux.

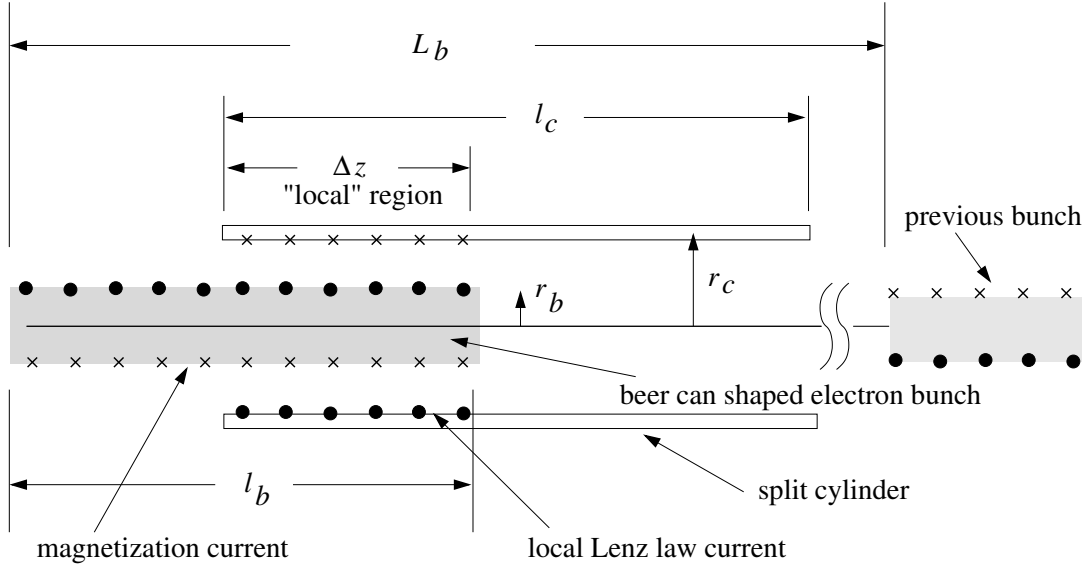


Figure 5: Schematic of beer-can-shaped electron bunch entering the split-cylinder resonator, which is longer than the bunch. Lenz's law is applied to the local overlap region of length Δz . Flux due to the induced Lenz law current is assumed to exactly cancel locally the flux due to the Ampère bunch polarization current.

The Lenz law magnetic field is $B_{LL} = \mu_0 i_{LL}$ and the magnet flux through the cylinder is

$$\phi_{LL} = \mu_0 \pi r_c^2 i_{LL}. \quad (6)$$

According to Jackson's[4] section 5.10, the magnetic field \mathbf{B}_b within the polarized beam bunch is equal to $\mu_0 \mathbf{M}_b$ which is the magnetization (magnetic moment per unit volume) due to the polarized electrons.

$$B_b = \mu_0 M_B = \mu_0 \frac{N_e \mu_B}{\pi r_b^2 l_b}, \quad (7)$$

where N_e is the total number of electrons in each bunch. The flux through ring thickness Δz of this segment of the beam bunch is therefore

$$\phi_b = B_b \pi r_b^2 \Delta z = \mu_0 \frac{N_e \mu_B}{l_b} \Delta z, \quad (8)$$

which is independent of bunch radius r_b . Since the Lenz law and bunch fluxes have to cancel, from Eqs. (6) and (8) we obtain

$$i_{LL} = -\frac{N_e \mu_B}{l_b} \frac{1}{\pi r_c^2}. \quad (9)$$

For a bunch that is longitudinally uniform (as we are assuming) we can simply take Δz equal to bunch length l_b to obtain

$$I_{LL} = i_{LL} l_b = -\frac{N_e \mu_B}{\pi r_c^2} \frac{\Delta z}{l_b}. \quad (10)$$

Once the bunch is fully within the cylinder, I_{LL} “saturates” at this value.

We now make the further assumption (somewhat contradicting the figure, but consistent with the proposed J-LAB test) that the bunch is sufficiently shorter than the cylinder (i.e. $l_b \ll l_c$) that the linear build up of I_{LL} can be ascribed to a constant applied voltage V_{LL} required to satisfy Faraday’s law.

For a CEBAF $I_e = 160 \mu\text{A}$, 0.5 GHz bunch frequency beam the number of electrons per bunch is approximately 2×10^6 . Using parameters from Table 1 we obtain the maximum Lenz law current to be

$$I_{LL}^{\text{max.}} = -\frac{N_e \mu_B}{\pi r_c^2} \quad \left(\text{e.g. } -5.9078 \times 10^{-14} \text{ A} \right). \quad (11)$$

There will be an equal excess charge induced on the capacitor during the bunch exit from the cylinder, at which time the resonator phase has reversed. The total excess charge that has flowed onto the capacitor due to the bunch passage is

$$Q_1^{\text{max.}} \approx I_{LL}^{\text{sat.}} \frac{l_b}{v_e} \quad \left(\text{e.g. } -3.2312 \times 10^{-24} \text{ C} \right). \quad (12)$$

Depending, as it does, on the bunch charge profile, and the ratio of bunch length to cylinder length, this result is expressed only as an approximation. The meaning of the superscript “max” is that, if there were no further resonator excitations, the charge on the capacitor would oscillate between $-Q_1^{\text{max.}}$ and $+Q_1^{\text{max.}}$. All that remains to do is to confirm the perfectly-constructive, coherent build-up indicated in Figure 4, and to calculate the factor by which this maximum capacitor charge has increased when steady-state circuit response has been reached.

Comparison of different signal levels in a consistent way in this paper will be referenced to the energy transferred to the capacitor during a single bunch passage through the resonator. The energy transfer from the beam polarization signal just analysed will be designated $U_1^{\text{pol.}}$. This is the “foreground” quantity that, magnified by a resonant amplitude magnification factor M_r^2 will provide the actual polarization measure in the form of steady-state energy $U^{\text{pol.}}$ stored on the capacitor;

$$U^{\text{pol.}} = \frac{1}{2} \frac{Q_1^{\text{max.}2}}{C_c} M_r^2 \sin \psi = \left(M_r^2 \times 1.0899 \times 10^{-35} \text{ J} \right) \sin \psi \quad (13)$$

where, as calculated in Eq. (12), $Q_1^{\text{max.}} = 3.2312 \times 10^{-24} \text{ C}$ is the charge deposited on the resonator capacitance during a single bunch passage of a bunch with the nominal ($N_e = 2 \times 10^6$ electrons) charge. The final $\sin \psi$ factor is an arbitrary phase factor that will be explained later, in connection with synchronous detection. This equation is boxed to emphasize the importance of $U^{\text{pol.}}$ both in absolute terms and for relative comparison with “background”—another excitation source, which causes spurious capacitor energy changes, will later also be boxed.

Except for the back voltage due to charge accumulating on the capacitor, I_{LL}^{max} is the constant current that would flow in the inductance while a single bunch remains within the cylinder. But, because the resonator natural frequency is so high, it has not been quite legitimate to neglect the back voltage. As Figure 4 indicates, by the time the bunch exits the cylinder, the capacitor voltage is supposed to be just reversed. The transit time is

$$\Delta t = \frac{l_c}{v_e} \quad \text{e.g.} \quad \frac{0.04733}{2.596 \times 10^8} = 0.1823 \text{ ns}, \quad (14)$$

for which the transit cycle advance is $f_c \Delta t = 0.5$. As a result the (now reversed sign) Lenz law e.m.f. during the exit doubles the amount of charge that, in effect, has been allowed to bypass the inductance, to appear on the capacitor.

In a lumped constant circuit model $Q_1^{\text{max.}}$ is the (maximum during resonant cycle) excess charge on the capacitor due to the passage of a single bunch. Without subsequent bunch passages this

maximum charge would decay exponentially with time constant $2Q/\omega_c$, where Q is the resonator “quality factor”, and ω_c is the natural frequency of the resonator.

As Figure 4 also indicates, the parameters have been adjusted so that all bunch entrances and exits contribute constructively to Q^{\max} . On subsequent bunch passages there will already be current flowing due to previous bunch passages. Eventually a steady state will be achieved, in which the resonator energy gained during each bunch passage exactly cancels the ohmic energy lost during the interval between bunch passages.

4 Foreground magnetization excitation calculation

When a longitudinally polarized bunch enters the conducting cylinder its magnetization tries to change the flux linking the cylinder. By Lenz’s law this change in flux is opposed by azimuthal current flowing in the cylinder. After many cycles a steady state is established in which the induced response each cycle just matches the resistive decay of the resonator.

In any case the Lenz law current is present only while the bunch is passing through the cylinder. It is a quite good approximation to treat the applied voltage as having a two square “top hat” shapes, one sign at entry, the opposite sign at exit. For the circuit to respond to beam magnetization, but not to the charge itself, the bunch magnetizations alternate, pulse-to-pulse. This is accomplished by merging a longitudinally polarized “A” beam with an oppositely-polarized and half-period-time-displaced, but otherwise identical “B” beam. Correspondingly, the resonator is tuned to an odd harmonic of the combined A+B beam frequency divided by 2.

The effect of the pulse-to-pulse alternation of the polarization is to reduce the (current-weighted) polarization frequency from 0.5 GHz to 0.25 GHz. Odd harmonics of 0.25 GHz that are excited by the beam polarization will therefore be isolated in the frequency domain from direct charge excitation at harmonics of 0.5 GHz.

In actual practice, as well as having alternating polarization, the A and B bunch charges will not be exactly equal, which will cause some direct charge excitation to leak into odd harmonics. However this spurious signal will also be reduced by careful alignment and positioning of the polarimeter configuration to take advantage of its symmetry. Further selectivity enabled by modulation will be described later.

In a MAPLE program used to calculate the response, the excitation is modeled using a “piecewise defined” train of pulses. The bipolar pulses modeling entry to and exit from the resonator are obtained as the difference between two “top hat” pulse trains, one slightly displaced from the other in time. Here is a fragment of this code:

```
TopHatAltWave0 := t-> piecewise(
    0<t and t< 0+1.,      1,
    1*h_c<t and t< 1*h_c+1, -1,
    2*h_c<t and t< 2*h_c+1,  1,
    3*h_c<t and t< 3*h_c+1, -1,
    4*h_c<t and t< 4*h_c+1,  1,
    .....
    53*h_c<t and t< 53*h_c+1, -1,
    54*h_c<t and t< 54*h_c+1,  1,
    55*h_c<t and t< 55*h_c+1, -1,
    56*h_c<t and t< 56*h_c+1,  1, 0):
    .....
TopHatAltWaveDiff := t-> TopHatAltWave0(t) - TopHatAltWave0p3(t):
```

The last line shows the subtraction of a wave displaced by 0.3 time units (the earlier excerpt show a few lines) from an identical, but undisplaced train.

In this form the bipolar pulse separations are 1 unit and the bunch-to-bunch separations are 11 units. (The choice of 11 is based on the tentatively adopted harmonic number $h_c = 11$, which is the ratio between resonator frequency and (same polarity) bunch frequency.) Two short sections of the top hat pulse train are shown in Figure 6.

The bunch train (as modeled in the program) terminates after, for example, $\mathcal{Q} = 1000$ pulses, (where \mathcal{Q} is the resonator quality factor) by which time a steady state has almost been achieved. This enables the complete analysis, including transients, to be performed by Laplace transformation. But, to satisfy Laplace transform requirements, the excitation has to terminate at finite time. An alternate approach, that would suppress transients and keep only the steady-state response, would be to represent the bunch train by a Fourier series and to use the complex impedance formalism.

As explained in a later figure caption, in order to reduce the computation time (and avoid saturating the figure data sets) the circuit resistance has been artificially increased by a factor of about 10, $r_c \rightarrow 10r_c$. This only affects the figures. The actual excitation is obtained from the analytic formulas described next.

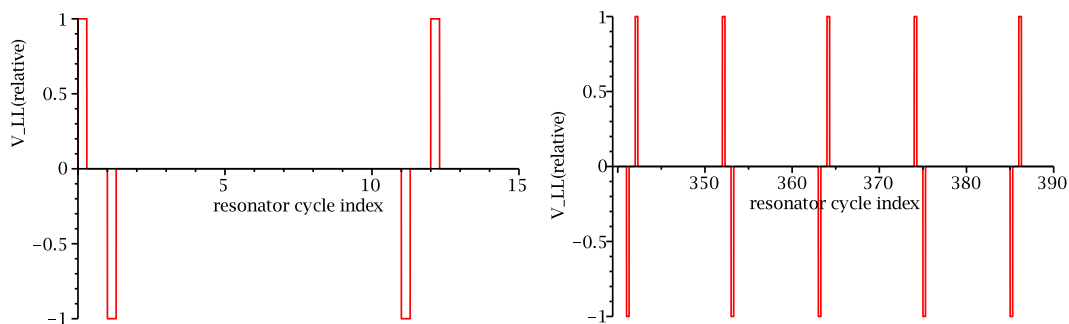


Figure 6: Pulsed excitation voltage pulses caused by successive polarized bunch passages through the resonator. A few initial pulses are shown on the left, some later pulses are shown on the right. The units of the horizontal time scale are such that, during one unit along the horizontal time axis, the natural resonator oscillation phase advances by π . The second pulse starts exactly at 1 in these units, because the resonator length l_c has been arranged so that this time interval is also equal to the bunch transit time through the split-ring. Also, $h_c=11$ units of horizontal scale advance corresponds to a phase advance of π at the $f_A = f_B = f_0 = 0.2495$ GHz “same-polarization repetition frequency”. In other words, 1 unit corresponds almost exactly to $2/11$ ns time duration and is a phase advance of π at the $h_c f_0$ polarization repetition frequency and 2π at the $2h_c f_0$ charge repetition frequency.

Lumped constant representation of the split-cylinder resonator as a parallel resonant circuit is shown in Figure 7. The resistor symbol is lower case r as mnemonic reminder that we are dealing with a circuit for which inductance L and capacitance C are dominant. The resistor r is taken in series with the inductance under the assumption that the resistance of the inductance dominates all other circuit losses (including, for example, dielectric losses).

The element impedances are given in the figure. The excitation caused by polarized beam passing through the split-cylinder is represented by Lenz law voltage source \bar{V}_{LL} , which is the alternating bunch train already described. Voltage division in this series resonant circuit produces capacitor voltage transform $\bar{V}_C(s)$;

$$\bar{V}_C(s) = \frac{1/(Cs)}{1/(Cs) + r + Ls} \bar{V}_{LL}(s) = \frac{\bar{V}_{LL}(s)}{1 + rs + CLs^2}. \quad (15)$$

For excitation voltage $V_{LL}(t)$ as shown in Figure 6, MAPLE has been used to determine the Laplace transform $\bar{V}_{LL}(s)$ for substitution into this equation, to obtain $\bar{V}_C(s)$. Input pulses and equilibrium response, obtained using MAPLE to invert the transform are plotted in Figure 8. The capacitor voltage $V_C(t)$ is plotted in Figures 9 and 10.

This comparison shows that the response is very nearly in phase with the excitation.

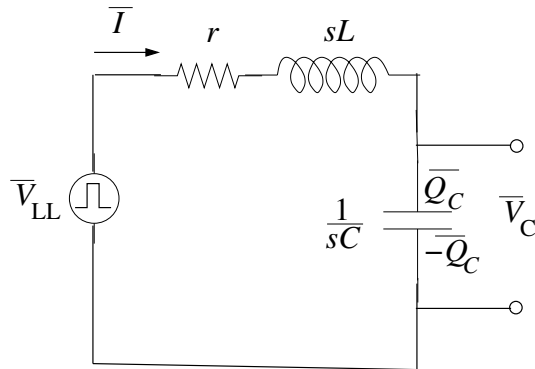


Figure 7: Circuit model for excitation voltage division between capacitance C and inductance L of the resonant LC . The overhead bars on the \bar{I} \bar{V} symbols indicate they represent Laplace-transformed circuit variables.

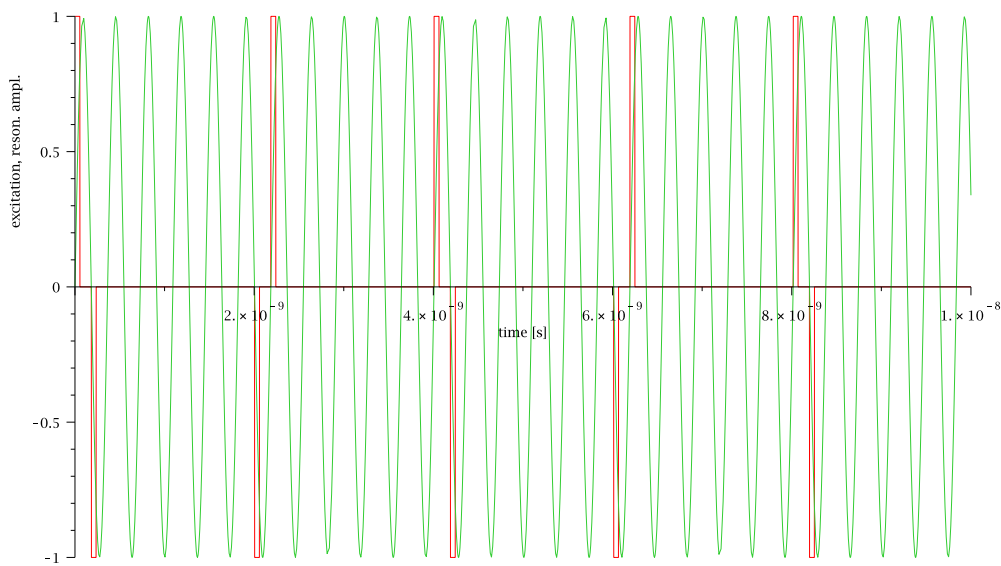


Figure 8: Alternating polarization excitation pulses superimposed on resonator response amplitude and plotted against time. Bunch separations are 2 ns, bunch separation between same polarization pulses is 4 ns. The vertical scale can represent V_C , E_ϕ , dB_z/dt , or dI_C/dt , all of which are in phase.

5 Background resonator excitation by bunch charge

The alternating polarization of successive bunches moves the polarimeter resonant frequency away from harmonics of the bunch frequency. But the A and B bunch currents will not be exactly equal, causing the beam charge to have a residual component with frequency equal to the natural resonator frequency and capable of producing resonant build-up.

The electromagnetic fields of the split-cylinder resonator are quite simple. The magnetic field

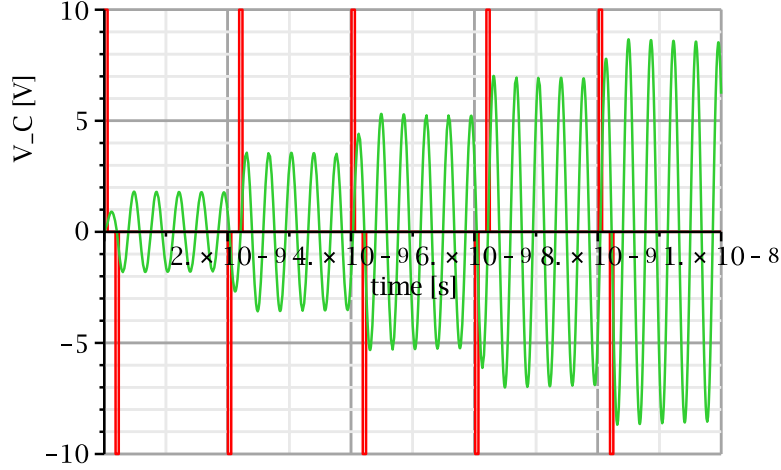


Figure 9: Accumulating capacitor voltage response V_C while the first five linac bunches pass the resonator. The accumulation factor relative to a single passage, is plotted.

shape, even at microwave frequency, is very nearly the same as the low frequency shape given by magnetostatics—uniform B_z in the interior, with return flux outside the cylinder.

(After almost instantaneous re-establishment of steady state) the current distribution induced by bunch magnetization is purely solenoidal; and the vector potential from a purely solenoidal current distribution is also purely solenoidal. It follows also[5] that, even for a time-varying solenoidal field, the electric field is purely radial—the only non-vanishing electric field component is the radial component E_r , present as a consequence of Faraday’s law. In the fringe field region there is also a non-zero radial magnetic field component B_r . But, by symmetry (with effect of sliced cylinder neglected) $B_\phi = 0$ everywhere.

As a cylindrical waveguide open at both ends, the cylinder can also resonate at frequencies above waveguide cut-off. But, with cylinder radius r_c only 1 cm, all such resonances can be neglected—their frequencies are well above the highest value of f_c under consideration.

To calculate the interaction of the charged bunch with the resonator we therefore need only consider the B_z , B_r and E_r components. Furthermore, even the B_z and B_r components can be neglected—they deflect the bunch but, to first approximation, as shown below, they cause no energy transfer between bunch and resonator. For these reasons we can treat the orbits through the resonator as curvature-free straight lines.

To estimate the importance of direct charge, background excitation we can assume steady-state resonator response at the level calculated for the foreground bunch magnetization response, and calculate the additional transient excitation of the resonator due to the Faraday’s law electric field acting on the bunch charge. Eq. (12) gives the maximum charge on the capacitor after a single bunch passage to be $Q_1^{\max} = 3.231 \times 10^{-24}$ C, which builds up by a factor of $Q/h_c = 730$ to a saturation level of $Q_C^{\text{sat.}} = 2.080 \times 10^{-21}$ C. From this value, and the “impedance ratio”, $Z_c = \sqrt{L_c/C_c} = 121.08$ ohm, the saturated inductance current can be calculated;

$$I_L^{\text{sat.}} = \frac{V_C^{\text{sat.}}}{Z_c} = 3.587 \times 10^{-11} \text{ A.} \quad (16)$$

The corresponding maximum magnetic field is solenoidal, with value

$$B_c^{\text{sat.}} = 0.9522 \times 10^{-15} \text{ T.} \quad (17)$$

This is a very small magnetic field, but it is oscillating at very high, 2.74 GHz frequency, and with essentially perfect regularity. By conventional spectral analysis, this makes the induced magnetic field

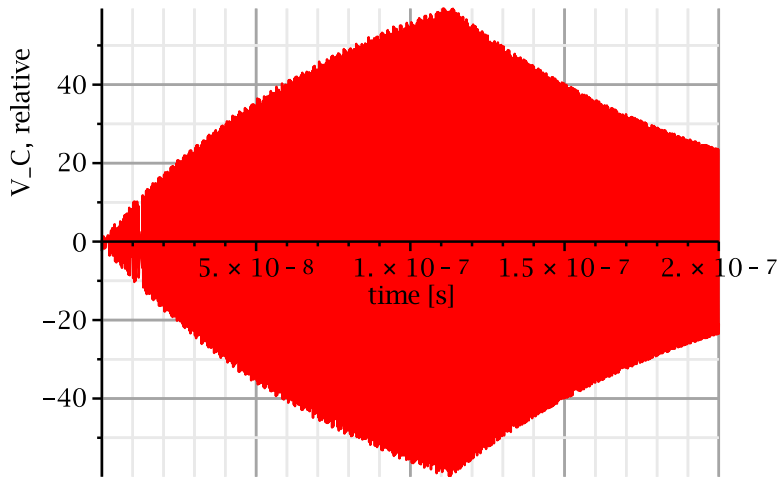


Figure 10: Relative resonator response to a train of beam pulse that terminates after about 110 ns. (The Laplace transform formalism requires the time duration of the excitation to be finite.) After this time the resonator rings down at roughly the same rate as the build-up. With just one exceptions the circuit parameters are those given in Table 1. The exception is that the resistance for the plot is $r = 10r_c$. The true response build up would be greater by a factor of 10, over a 10 times longer build-up time.

measurably large. Here, though, the task is to calculate the work done on a bunch caused by the corresponding Faraday’s law electric field along with cavity misalignment.

At DC there would be no work done by such a magnetic field on a charged particle. But we are dealing with a time varying magnetic field. In fact, the time variation has been intentionally arranged to reverse the magnetic field during the transit time through the split-cylinder. Like the magnetization response, any energy transfers from particle to resonator have the potential for either adding constructively or destructively.

The thin gap in the cylinder is essential for enabling high Q resonance but, otherwise, its presence does not significantly influence excitation on short time scales. This has already been exhibited in the calculation of resonant excitation by beam magnetization, and the same simplification applies for direct charge sources. The validity of neglecting the gaps is enhanced by arranging them symmetrically, as shown in Figure 12.

5.1 Off-axis, parallel particle incidence

Consider a beam bunch approaching the solenoid parallel to the cylinder axis (continuing to treat the gap thickness g_c as negligible). There is no significant energy transfer from beam to resonator occurring inside the resonator cylinder—magnetic fields do not change particle energy and the Faraday’s law electric field E_r is transverse and does no work. We need, though, to calculate particle energy changes induced in the fringe field regions. The longitudinal magnetic field can be expressed as $B(z)\hat{\mathbf{z}}$ where $B(z)$ varies from $B(z-) = 0$ well before entry to $B(z+) = B_0$, well inside the cylinder. The full magnetic field, in linearized approximation, is

$$\mathbf{B} = \frac{-dB(z)/dz}{2} \Big|_{\text{on-axis}} (x\hat{\mathbf{x}} + y\hat{\mathbf{y}}) + B(z)\hat{\mathbf{z}}, \quad (18)$$

where $B(z)$ is a function varying over a short z -interval, from a constant value of 0 outside to a value of B_0 inside. The $\nabla \cdot \mathbf{B} = 0$ vanishing divergence condition can be seen to be satisfied. The function

dB_z/dz is strongly peaked at the solenoid entrance and exit, and can be approximated by the sum of two δ -functions. As a result

$$B_x(z) = B_y(z) = -\frac{1}{2} \frac{dB_z}{dz} \approx \frac{-B_0}{2} \left(\delta(z + l_c/2) - \delta(z - l_c/2) \right), \quad (19)$$

where B_0 is the constant, longitudinal, magnetic field inside the cylinder. An electron initially traveling in the horizontal $y = 0$ design plane, along a line at constant $x = \Delta x$, impulsively acquires an azimuthal (vertical) velocity Δv_y at the entrance satisfying

$$m_e \gamma_e \Delta v_y = \int_{-l_c/2}^{-l_c+/2} e v_e \hat{\mathbf{z}} \times B_x(z) \hat{\mathbf{x}} \Big|_y dt = \int_{-l_c-/2}^{-l_c+/2} \frac{B_0}{2} \delta(z + l_c/2) d(v_e t) = \frac{e B_0}{2}. \quad (20)$$

This agrees with Kumar's Eq. (5)[6]. Solving this equation for Δv_y with resonant split-ring resonator parameters, the vertical angle $\Delta\theta_y$ is given by

$$\begin{aligned} \Delta\theta_y &= \frac{\Delta v_y}{v_e} = \frac{c B_c^{\text{sat.}}}{2 \beta_e \gamma_e m_e c^2 / e} \Delta x \\ &= \frac{(3 \times 10^8)(10^{-15})}{(2)(0.866)(2)(0.511 \times 10^6)} \Delta x \\ &= 1.7 \times 10^{-13} \Delta x. \end{aligned} \quad (21)$$

This radial deflection initiates a helical motion, but the particle stays in the cylinder only for a time of duration l_c/v_e , which is not long enough for any significant motion other than in the y -direction to develop.

The extreme smallness of the coefficient in Eq. (21) is due to the extremely weak induced magnetic field factor. One sees that the work on any particle entering the solenoid parallel to the cylinder axis, can be neglected, irrespective of its transverse position. The value of $\Delta\theta_y$ given by Eq. (21) can be compared with the same angle $\Delta\theta_y$, arising from equipment misalignment errors. Inescapable misalignment errors will inevitably cause angular orbit error much greater than the value given in Eq. (21).

5.2 Canted particle incidence

Resonator excitation resulting from non-zero angle of approach (to be referred to here as ‘‘cant angles’’) is considered in this section. As in the treatment so far, except for the small cant angle under discussion, the orbital azimuth can be taken to be horizontal without essential loss of generality, because of azimuthal symmetry.

Due to resonator misalignment or beam steering errors the beam centroid may enter the split-cylinder with canted angle, not parallel to the cylinder axis. Without loss of generality we can assume this angle is, say, vertical, $\Delta\theta_y$. The analysis in the previous section has shown that we can neglect any impulsive azimuthal velocity change occurring in the end field region. If the horizontal entry displacement Δx is zero, there will be no solenoidal transverse component of velocity and no work will be done. So we also assume $\Delta x > 0$.¹

¹Representing the entire bunch as if it is all situated at its centroid is tantamount to neglecting the transverse extent of the bunch and assuming the bunch radius is less than its displacement from the origin. Technically, this assumption becomes invalid once the bunch displacement is less than the bunch radius, which will always be the case once the line is properly tuned up. But the approximation actually remains good even in this limit, especially with the beer-can bunch shape. The displaced bunch can be replaced by a perfectly centered circular distribution (which does no work) plus two ‘‘lunes’’ (i.e. new-moon-shaped crescents) one with positive charge density, one negative. The fraction of total charge in each lune is approximately $\Delta x/r_c$. Representing each lune by a point at $x = r_c$ magnifies the work by a factor of roughly $0.5r_c/\Delta x$, compared to its being located at $x = \Delta x$. The work done on the two lunes is twice the work on the positive density one. All of this is equivalent to pretending $r_c \ll \Delta x$, in spite of the fact that r_c is actually greater than Δx .

For simplicity we also suppose the orbit is aimed vertically to cross the horizontal design plane $y = 0$ at the longitudinal $z = 0$ center of the resonator at time $t = 0$. The equation of the orbit path through the resonator is then

$$\begin{aligned} x &= \Delta x, \\ y &= -\Delta\theta_y z = -\Delta\theta_y v_e t, \end{aligned} \quad (22)$$

where v_e is the particle's (almost exactly longitudinal) velocity. Meanwhile, using Faraday's law, the solenoidal magnetic field, magnetic flux φ through a centered circle of radius Δx and the corresponding e.m.f. are given by

$$\begin{aligned} B_z &= B_c^{\text{sat.}} \sin(\omega_c t + \psi), \\ \varphi &= \pi \Delta x^2 B_c^{\text{sat.}} \sin(\omega_c t + \psi), \\ \text{e.m.f.} &= -\frac{d\varphi}{dt} = -\pi \Delta x^2 B_c^{\text{sat.}} \omega_c \cos(\omega_c t + \psi) \end{aligned} \quad (23)$$

where, for example, ω_c corresponds to the $h_c f_0 = 2.7$ GHz frequency with which the resonator is oscillating and ψ is a possible phase shift of the particle bunch arrival time relative to the resonator phase. The time dependence of B_z has been expressed as $\sin(\omega_c t + \psi)$ (rather than cosine) because B_z is "in quadrature" (when one is zero, the other is maximum or minimum) with, for example, V_c , which can be seen in Figure 8 to be sine-like at the time origin. (More on the phase issue later.) The beam bunch is subject to a Faraday's law electric force given by

$$F_y = N_e e E_\phi = N_e e \frac{\text{e.m.f.}}{2\pi \Delta x} = -\frac{1}{2} N_e e \Delta x B_c^{\text{sat.}} \omega_c \cos(\omega_c t + \psi). \quad (24)$$

(With the vertical motion being non-relativistic) the work done on the bunch during vertical displacement $v_e \Delta\theta_y dt$ is $dW^{\text{m.a.}} = F_y v_e \Delta\theta_y dt$ and the total work done during a single bunch passage is given by

$$W_1^{\text{m.a.}} = -\frac{1}{2} \frac{N_e e \omega_c}{\omega_c} v_e \Delta\theta_y \Delta x B_c^{\text{sat.}} \int_{-\pi/2}^{\pi/2} \left(\cos \omega_c t \cos \psi - \sin \omega_c t \sin \psi \right) d(\omega_c t). \quad (25)$$

The integral evaluates to $2 \sin \psi$ and, instead of canceling out the ratio ω_c/ω_c , it can be replaced by $2f_0/2f_0$ to permit the factor $N_e e 2f_0$ to be replaced by the proposed average injection line beam current of $160 \mu\text{A}$. The current imbalance can then be expressed as a fractional deviation $\Delta I_{\text{ave}}/I_{\text{ave}}$ since, with perfect tuning, the operative frequency component of beam current will vanish.

$$\boxed{W_1^{\text{m.a.}} = \left(\frac{\Delta I_{\text{ave}}}{2f_0} v_e B_c^{\text{sat.}} \frac{1}{r_c} \right) \left(\Delta\theta_y \Delta x \right) \sin \psi' = \left(4.5 \times 10^{-20} \text{ J/m} \right) \left(\frac{\Delta I_{\text{ave}}}{I_{\text{ave}}} |\rho| \Delta\theta_\perp \right) \sin \psi'.} \quad (26)$$

In the final equation the factor $\Delta\theta_y \Delta x$ has been replaced by $|\rho| \Delta\theta_\perp$, where (temporarily) expressing $|\rho|$ redundantly as absolute value is only to emphasize that cylindrical coordinate radius coordinate ρ , is positive by convention, and has replaced Δx . Also θ_\perp has replaced $\Delta\theta_y$. Note, though, that the expression is "quadratically small" in that, except for misalignment errors, ρ and $\Delta\theta_\perp$ would each vanish separately.

These calculations have exploited azimuthal symmetry (which, strictly speaking, is valid only to the extent it is valid to neglect the azimuthal location of the gap for time durations short enough for the gap capacitance to be treated as a short circuit). The validity of this approximation, with multiple resonant cells, depends on the gap azimuthal locations averaging to zero. This means there have to be at least two resonant cells, for example as shown in Figure 11.

The arbitrary phase-dependent factor $\sin \psi'$ in Eq. (26) is like the $\sin \psi$ factor introduced earlier in Eq. (13). Until now, ψ and ψ' have been independent parameters. If and when a relation between

ψ and ψ' has been obtained this will no longer be true. Also the negative sign in Eq. (26) has been recognized as an arbitrary phase factor and dropped.

Like Eq. (13), Eq. (26) is boxed to emphasize the importance of comparing “background” $W_1^{\text{m.a.}}$ with “foreground” $U^{\text{pol.}}$. The superscript on $W_1^{\text{m.a.}}$ is an abbreviation for “misalignment”. With perfect, time-independent positioning of the resonator, $W_1^{\text{m.a.}}$ would vanish, but this would clearly be unrealistic in general.

The presence of phase factors in the boxed equations makes it advisable to investigate whether phase sensitive detection can be used as an aid in distinguishing foreground from background. It will be important to analyse whether ψ and ψ' can be chosen to be the same (meaning the background and foreground are “in phase”, or differ by an odd multiple of $\pi/2$, in which case, except for arbitrary sign, foreground and background would be “in quadrature”).

6 Synchronous signal processing

6.1 Coherent summation of resonator outputs

Because the magnetization-induced resonator excitation is so weak it will be advantageous to be able to coherently add the excitation amplitudes from more than one, for example, let us say, $N_d = 4$ or 8 separate transducers. This permits the restoration of azimuthal symmetry to the polarimeter, by symmetrizing the cylinder slice orientations. With the separate resonator signals coherently summed, there is a single polarimeter output signal to deal with, which contains both foreground and background contributions.

The alternating polarization of successive bunches has already provided one stage of background rejection by “eliminating” the beam current frequency content at all odd harmonics of f_0 , while assuring that the magnetization spectrum consists of all harmonics of f_0 and, in particular, the background-free odd harmonics.

A schematic physical representation of the proposed apparatus is shown in Figure 11. Readout circuitry is shown in Figure 12. The apparatus has been designed both for signal magnification and for enhanced foreground/background separation. Signals are combined without reflection in the combiner. (Direct connection of the resonator outputs to a common transmission line would load the resonators unacceptably.) Optimally designed loop coupling limits the loading by inductively coupling out the optimal amount of energy from the resonators. As indicated in Figure 2, the effective “turns ratio” of this coupling is proportional to the fraction of the return flux (which is equal to the flux through the cylinder) that is intercepted by the inductive loop. This fraction depends on the characteristic impedance of the transmission line. The purpose is to present adequately high impedances to the resonators, but with output impedance matched to the transmission line impedance. A lumped-constant circuit calculation will be provided shortly.

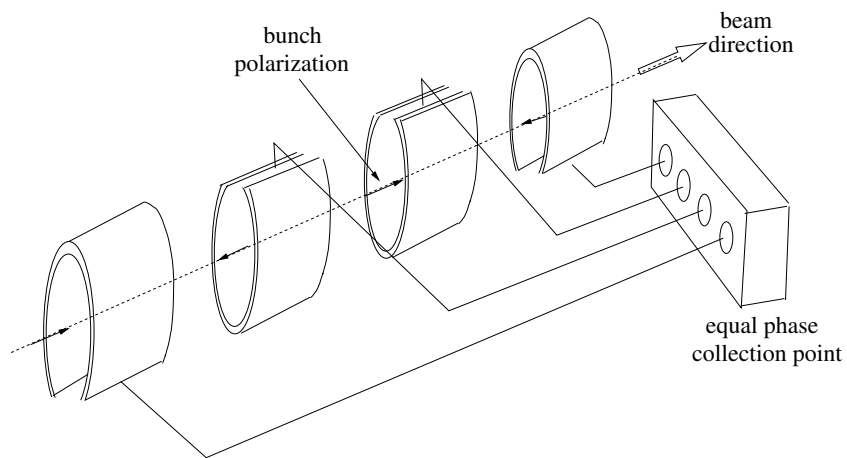


Figure 11: Sketch showing beam bunches passing through multiple resonators. With cylinder gaps up or down, the horizontal beam position (but not slope) sensitivity vanishes by symmetry. With gaps arranged down-up-up-down, the vertical position (but not slope) sensitivity also vanishes. Cable lengths are arranged so that beam bunch current (not polarization) signals exactly cancel. To the extent the bunch polarization alternation is imperfect, the resonators will still therefore give non-zero direct charge response for canted-bunch trajectories through the resonators. This response will be suppressed by a combination of (i) steering beam parallel to (average) resonator axis, (ii) beam centering and (iii) differential modulation to separate foreground and background signal frequencies. Most of these measures also tend to cancel errors due to imperfect internal resonator positioning.

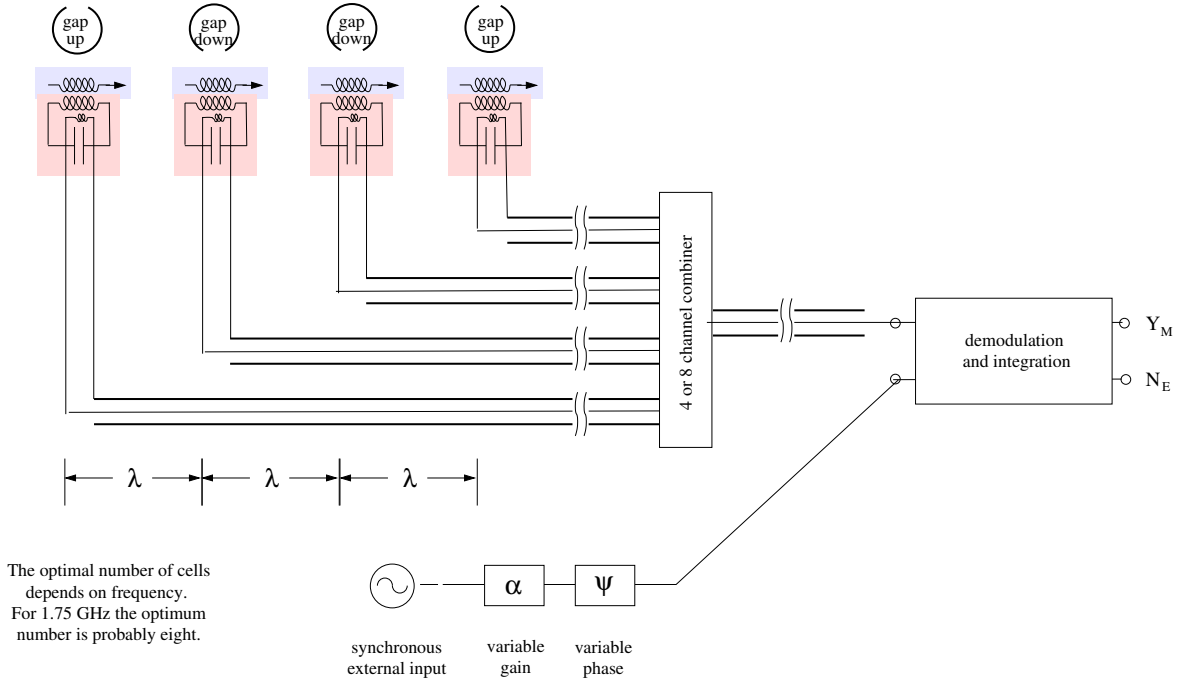


Figure 12: Circuit diagram for a circuit that coherently sums the signal amplitudes from four polarimeter cells. (For $h_c = 7, 9, \text{ or } 11$, there will actually be eight cells, as appropriate for a roughly meter-long polarimeter.) Excitation by passing beam bunches is represented by inductive coupling, with the coupling ratio set for maximum power extraction. The resonant frequency for each cell might be set, for example, to $f_c = 1.7465 \text{ GHz}$ (lower by the factor $7/11$ than the frequency assumed in previous graphs). Ideally, with perfect alignment, tune-up, and electronic processing, foreground excitation will appear at the Y_E (“Yes it is magnetic-induced”) output, and background excitation will appear at the N_E (“No it is electric-induced”) output. The external coherent signal processing functionality to achieve this separation is indicated schematically by the box labelled “demodulation and integration”. The demodulation function is to separate foreground from background, both of which have to compete with thermal noise. The integration function is to suppress thermal noise. Over sufficiently long runs, synchronous detection and processing can, in principle, accomplish both purposes, so that the foreground excitation appears at Y_E and the background at N_M . For set-up test purposes the B beam could be turned off, leaving only the A beam (unpolarized, for example). This excitation would exactly mimic ideally-tuned-up foreground, and should produce output appearing at Y_M .

6.2 Why synchronous detection? Why helicity matters?

Previous sections have validated ignoring the angular deflection of the particle orbits caused by the resonator magnetic field on the particle itself—though actually following a very slightly helical orbit, each particle, and therefore also the bunch centroid, can be treated as following a straight line through the split-cylinder. However angular deviations from zero due to element misalignment cannot be neglected. *The sign of the instantaneous work being done on a particle by the resonator boils down to the question of whether the dot product of the Faraday’s law electric field vector with the particle’s velocity vector is positive or negative.* (Because the Faraday’s law electric field vector is exactly azimuthal) this boils down to whether the “effective helicity” of the particle (or bunch centroid) is positive or negative. Here “effective helicity” is an ad hoc (temporary) property describing whether the particle trajectory is related to the resonator axis as a left-hand or a right-hand screw. (If, viewed with particle approaching, the particle line is sloping up as it misses the resonator axis on the right, then the particle advance is like that of a right-hand screw, etc.)

A possible background suppression mechanism relates to the phase-dependent factors appearing in boxed Eqs. (13) and (26). These $\sin \psi$ and $\sin \psi'$ factors have been referred to as “random phase factors”. Especially at GHz frequencies, it is hard even to define such phase angles. It is only rarely possible to measure such phases in practice. As a practical matter, it is only easy to measure the phase difference $\Delta\psi$ between two sinusoidally-varying amplitudes being measured at the same location.

As it happens, our apparatus, which responds synchronously to foreground (magnetization-excitation) and background (charge-excitation) is one such instance. This detection sensitivity would *not* be essential under perfect beam conditions, in which the charge excitation is limited to even harmonics of f_0 , and the resonator is tuned to an odd harmonic of f_0 . Rather, we are concerned with improperly balanced A and B bunches which leads to charge excitation at odd harmonics of f_0 —in particular the odd harmonic to which the resonator is tuned.

Most accelerator beam position or beam current monitors are not capable of resolving quadrature components separately (for example because no absolute phase reference signal is available). But within the telecommunications field it is standard practice to resolve quadrature components. This does, however, require phase sensitive detection, which requires, in turn, a very stable trigger pulse train synchronized with the beam pulse arrival times. Such a stable reference frequency source will be available at the CEBAF injection line. This should make synchronous detection possible.

Figure 12 indicates this functionality schematically. By design the foreground magnetization-induced signal would appear at the Y_M (“yes, it is magnetic”) terminal, and the background charge-induced signal would appear at the N_E (“no, it is electric”) terminal. This will eventually be the case, but not without substantial further discussion, and signal processing refinement.

To analyse this issue one can consider the most extreme possible example of sub-harmonic beam current frequency leakage from $2f_0$ to f_0 . Let us suppose one or the other of the A and B beams is turned completely off, without affecting the other. On paper, this can be done exactly; we idealize by assuming it has been done to very high precision in the real world. Then the beam current frequency spectrum is purely sub-harmonic, at frequency f_0 and all of its harmonics—including, for example, the resonator natural frequency. In this configuration the background charge excitation caused by, say, the A beam, closely mimics the excitation of perfectly balanced, interleaved, opposite-polarization, A and B beams. Consider the passage through the resonator of such a beam bunch, and compare magnetization and charge excitation.

For the beam *magnetization* excitation to be maximal, the capacitor voltage V_C is zero as the bunch enters the cylinder (see Figure 8) and zero again as it leaves. At these points the inductor current is maximum. As the bunch passes the center point there will have been a 90 degree phase shift, and the inductor current will vanish. But the time rate of change of the inductor current, and therefore also the Faraday electric field, will be maximal.

The instantaneous coupling of bunch *charge* to resonator is proportional to the Faraday electric field. Under the same conditions as in the previous paragraph, at the same central instant, the charge coupling between bunch and resonator will also be maximal. Furthermore, since the energy transfer

does not change sign during passage through the cavity, the total work done in transit is maximal.

The conclusion to be drawn from the previous two paragraphs is that any non-zero-helicity charge coupling to the cavity is *in-phase* with the magnetization signal.

(Superficially) this seems unfortunate, in that it indicates that the dominant background error signal will show up at the Y_M output terminal, even though its source is the result of equipment misalignment rather than beam magnetization. This means that, for self-consistency, the phase factors in the boxed formulas have to be the same. That is, $\psi = \psi'$ in the boxed equations. This means that, even with synchronous detection, the signal appearing at the Y_M terminal in Figure 12 still contains background contamination. Formally, this also means that we may as well set $\sin \psi = \sin \psi' = 1$, since we are unable to exploit the possible difference of ψ and ψ' . The parenthetic “superficially” at the beginning of this paragraph will be justified in the next section, when *parameter modulation* is discussed as a way of separating foreground from background.

Digression: Our effort to measure the magnetization state of particle bunches is greatly simplified by the fact that the bunches contain 2×10^6 particles, passing at high and regular GHz repetition rate. Even with such large charge, it is difficult for the resonator magnetization excitation to be visible above the thermal noise floor. Our theoretical estimates so far make it clearly impossible to detect the excitation of any macroscopic resonator by the passage of a single electron. But, if the resonator were a single atom or molecule, it would presumably be possible for the interaction to be influenced by the electron’s helicity state. Of course this situation can only be analysed quantum mechanically. But, from the present classical treatment, it should not be surprising for the excitation to depend significantly on the electron helicity. This is the basis for the left-right scattering asymmetry of Mott-scattering polarimetry[8]. Regrettably, even apart from its destructive nature, the analyzing power of this form of polarimetry is woefully too weak for our beam polarization feedback goal.

7 Modulation-induced, foreground/background separation

So far we have only seen that our background and foreground signals are in-phase, *not* in quadrature. So synchronous detection cannot, as yet, enable the separation of background from foreground. Nevertheless, we continue to investigate ways in which synchronous detection can be exploited.

Based on our new emphasis of “effective helicity”, in order to better analyse background rejection, we refer again to Eq. (26). Though it is not conventional terminology, for mnemonic purposes, the quantity $\rho\Delta\theta_{\perp}$ is being referred to as “effective helicity”. (Recall that other angular misalignment, $\Delta\theta_{\parallel}$, parallel to the positional offset, causes no resonator excitation.) When the centroid is very nearly aligned, the effective helicity has been nulled very nearly to zero, but of one sign or the other. From this condition, the tiniest of steering changes causes the effective helicity to reverse, which causes the sign of the excitation to reverse. One wants to exploit this feature for tuning purposes.

Consider the following trigonometric identity, which is applicable to a situation in which a “carrier” signal of frequency ω is amplitude-modulated at frequency Ω :

$$\sin \omega t \sin \Omega t = \frac{1}{2} \left(\cos(\omega - \Omega)t - \cos(\omega + \Omega)t \right). \quad (27)$$

For our purposes, ω is a very high frequency, of order GHz, and Ω is a very low frequency, in the 1 Hz to 1 KHz range. One sees that the right hand side of the equation contains two, equal amplitude “side-bands”, oscillating at frequencies $\omega \pm \Omega$, shifted just slightly from ω . Viewed for a brief interval of time during which Ωt can be approximated as a constant phase shift, the sideband oscillations are “in quadrature” (and therefore separable) from the central frequency oscillation at frequency ω . But, as time evolves, the sideband phases shift relative to the central line and, over times longer than $2\pi/\Omega$, the side bands drift in and out of quadrature with respect to the central line.

Both frequencies, ω and Ω and both absolute phases, are under our external control, and they are synchronous with the linac bunch structure. With synchronous electronics capable of demodulating

the response by distinguishing background from foreground by frequency separation (and indicated by a box in Figure 12) we need only find ways to introduce differential modulation that modulates the foreground, but not the background, or vice-versa. Both possibilities are easily achieved.

The CEBAF operations group has already achieved low frequency modulation of the A and B bunch polarizations, without significantly altering the beam currents or other beam properties. For run durations of, say, one second, and perfectly stable bunch repetition frequency, a modulation frequency Ω_{pol} as small as ten Hertz will shift the foreground magnetization excitation to two measureably-distinct sideband signals, without affecting the charge frequency spectrum. Viewed on a spectrum analyzer, the center line would be due to the electric excitation, and the sidebands would be due to the magnetic excitation.

It is also possible to modulate the charge excitation without modulating the magnetization excitation. This was the motivation for emphasizing the “effective helicity” of the charge excitation. During set-up one will have reduced the effective helicity to best possible precision by careful beam steering. From this condition, by intentionally shaking the beam transversely at a “low” frequency Ω_{steer} , one will be modulating the background without modulating the foreground. In this case the central frequency will be magnetic and the side bands electric.

The latter, beam shaking, option may actually be the more powerful modulation procedure. Though polarization modulation is limited to the KHz range, beam shaking (through the extremely small angular range required) can be performed at high frequencies, in the MHz range. This would make it possible to modulate the frequency through a range large compared to the resonator bandwidth (which is given, for example, in Table 2) yet affecting the magnetization excitation hardly at all. This could be regarded as simply “sweeping away” the background excitation, by moving it outside the polarimeter-sensitivity frequency band. Basically the background charge excitation frequency would be changing too quickly for the resonators to “keep up”. This could reduce the background amplitude by a factor almost as great as the effective quality factor Q/h_c (also given in Table 2).

8 Circuit analysis

Forward and reverse impedance models for a single resonator are shown in Figure 13. It is assumed that each resonator will have a dedicated coaxial output connection. The coherent amplitude summing will be performed in the combiner shown in Figure 12. The circuit model follows Section 7.6 of the article by R. Berenger, contained in Montgomery, Dicke, and Purcell[7]. The output coupling is represented by a transformer with primary inductance L_c , secondary inductance L_L and mutual inductance M . Following Berenger, this transformer coupling is modeled by the T section shown. Approximate formulas for the circuit parameters are

$$\begin{aligned}
 L_L &= \mu_0 r_L \ln(8r_L/a_L - 1.75) \approx 1.021\mu_0 r_L, \\
 L_c &= \mu_0 \frac{\pi r_c^2}{l_c \mathcal{A}_{\text{corr}}}, \\
 M &= \frac{A_L}{A_2} L_c, \\
 C_c &= \text{determined by required resonant frequency } \omega_0,
 \end{aligned}
 \tag{28}$$

where the ratio of probe radius r_L to probe wire radius, r_L/a_L , has been taken to be 10. The correction factor $\mathcal{A}_{\text{corr}} = 1 + A_1/A_2$ corrects the split-cylinder inductance for the reluctance in the flux return path[1]. A_1 is the cross sectional area of the inner conducting tube, A_2 is the cross sectional area outside the inner tube and inside the outer. Though the applicable circuit parameters are given approximately by the simplified formulas given in earlier sections, the effective parameter values acquire correction factors to account for various effects. This is especially true for the split-cylinder capacity value C_c , which is especially sensitive because the gap width g_c is so small. The factor $\mathcal{A}_{\text{corr}}$ corrects the inductance for the reluctance of the flux return path. The effect of this correction is to

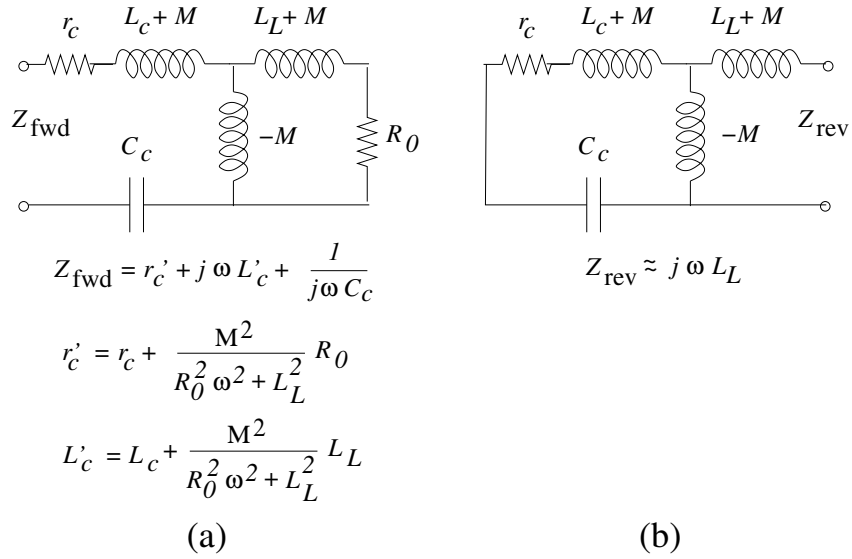


Figure 13: Forward (a) and reverse (b) impedance models for the loaded circuit. Primed quantities r'_c and L'_c can simply replace r_c and L_c to convert the unloaded model into the loaded model. With optimal output matching, $r'_c = 2r_c$; signal power estimates in Table 2 assume this optimal impedance matching. The reverse impedance is $Z_{\text{rev}} \overset{\text{e.g.}}{\approx} j 203 \Omega$. This is not large enough to permit any connection to the output (other than the impedance R_0 coax) without seriously mismatching the signal processing circuitry.

decrease the inductance, which increases the natural frequency. The effective parameter values are also influenced by the resonator loading caused by the output transmission line connection, as shown in the figure.

The desired resonant frequency is given by $\omega_c = 1/\sqrt{L'_c C_c}$ where L'_c is given in the figure. This makes it necessary to trim the capacitance C_c to give the required resonant frequency f_c . (A scheme for doing this has not yet been chosen.) For these reasons the gap capacitance parameters g_c and w_c given in parameter tables are somewhat unreliable; but the values for C_c itself should be more or less accurate.

9 Frequency choice considerations

The choice of harmonic number h_c , and therefore also of the resonator frequency has been left ambiguous so far. The section investigates this choice. The choice is strongly influenced by the possibility of increasing the signal strength by combining the signals from multiple resonators. The feasibility of doing this depends very much on the choice of resonator frequency. Especially at very low electron energies, the overall length of available beamline real estate restricts the length of apparatus that can be inserted in the beam line. This consideration greatly favors high frequencies, such as the $f_c = 2.7445$ GHz resonator frequency emphasized in the paper so far. (Higher frequencies, with $h_c > 11$, have been avoided for technical reasons, such as amplifier and bunch length limitations.)

Because the individual resonators are so short, especially at the highest frequency, it will be practical to line up several identical resonators, for example $N_{\text{cells}} = 8$, appropriately spaced, and let the beam pass through them in sequence. Assuming the resonators are physically identical, and identically aligned, their RF excitations will be identical. Added with perfectly constructive interference, the signal power would be increased by a factor $N_{\text{cells}}^2 = 64$. As well as improving the signal relative to thermal noise, a big signal amplitude increase like this also reduces the importance of extraneous noise

sources. Possible noise reduction measures that exploit the combination of equal signal amplitudes yet random thermal noise amplitudes have been thought of but not been seriously investigated.

Early sections of this paper have mainly taken $h_c = 11$ as the choice of harmonic number. To discuss the choice of frequency, parameters for other harmonic number choices, $h_c = 3, 5, 7, 9, 11$ are given in Table 2. This provides resonator frequency choices from $f_c = 0.74485$ MHz, to 2.7445 MHz. For any particular choice of frequency, the first parameter to be fixed is l_c , to match the transit time to the appropriate π phase advance. With cylinder radius r_c held constant, the inductance L_c is fixed, leaving the capacitance-sensitive parameters w_c and g_c as the only remaining free variables. (In fact even the presence of ring wall thickness w_c is artificial, in that using the parallel-plate capacitance formula is not at all accurate.) Except for this capacitance choice, fixing h_c essentially fixes all resonator parameters. With multiple resonators, the drift lengths scale proportionally. Even this requirement is not perfectly strict, since deviations could be compensated for by external cable lengths. (If the signals were summed by injecting them onto a single transmission line, external compensation could not be performed. But, in any case, as shown in Section 8, impedance reasons make it impractical to combine signals directly onto a common transmission line.)

The highest frequency case, $h_c = 11$, is optimal from some points of view, and especially for multiple resonator signal addition. With $N_{\text{cells}} = 8$ the overall length would be $L_{\text{tot.}} = 2N_{\text{cells}}l_c = 16 \times 0.04733 = 0.76$ m. Highest frequency can also be seen to be best for maximum resonator quality factor \mathcal{Q} . However the “effective \mathcal{Q} ” = \mathcal{Q}/h_c slightly favors low frequency. What causes this dependence is that the foreground power signal is proportional to $(\mathcal{Q}/h_c)^2$,

A parameter that is potentially important is the bandwidth f_c/\mathcal{Q} . In order for the gain of separate resonators to be the same it is important for their variation of natural frequencies to be negligible. Their spread of natural frequencies must be much smaller than this bandwidth.

It is not necessary, however, for modulation frequencies to be larger than f_c/\mathcal{Q} (which would typically be hard to achieve). Side-band frequency shifts caused by modulation only need to be significantly larger than is implied by the fractional r.m.s. spread of beam bunch arrival times, (which we continue to take to be zero). The bandwidth implied by the bandwidth times run-duration uncertainty product for a one second (or longer) run permits the effective detector band width to be as small as 1 Hertz (or smaller). The fact that f_c/\mathcal{Q} decreases with decreasing frequency is therefore not very important. To permit deferring the choice of harmonic number, parameters for all practical frequency choices are given in Table 2.

(These considerations would be different for polarized proton polarimetry, because of the much longer bunch lengths, and therefore greater resonator length, and lower frequency. Because of the frozen spin constraint, protons would have kinetic energy 234 MeV, and be much stiffer than the 0.5 MeV electrons considered in this paper, and also much more intense. In spite of these favorable considerations, achieving satisfactory resonant polarimetry for protons will probably require cryogenic resonators.)

10 Misalignment compensation budget

Of the two fundamental impediments to detecting the resonant beam magnetization signal, the one concerning isolation of signals from thermal noise is covered by the bottom two rows of Table 2. High frequency ($h_c = 7, 9, \text{ or } 11$) options are all favorable from the point of view of visibility relative to the thermal noise floor. The present section concentrates on the other fundamental impediment: the further suppression of charge-induced resonant background response, which could, otherwise, overwhelm the magnetization-induced foreground response.

Quantitative (boxed) formulas have been derived for both foreground, Eq. (13) and background

parameter harmonic numb.	symbol h_c	unit GHz	3	5	7	9	11
A,B bunch freq.	f_0	GHz	0.2495	0.2495	0.2495	0.2495	0.2495
resonant freq.	f_0	GHz	0.7485	1.2475	1.7465	2.2455	2.7445
dielectric			polyeth.	polyeth.	vacuum	vacuum	vacuum
rel. diel. const.	ϵ_r		2.30	2.30	1.00	1.00	1.00
numb. cells/m	N_{cell}	\approx /m	4	4	8	8	8
band width	f_c/Q	kHz	286	277	309	351	388
quality factor	Q		2.61e+03	4.51e+03	5.65e+03	6.40e+03	7.08e+03
effective qual. fact.	$M_r = Q/h_c$		8.72e+02	9.01e+02	8.07e+02	7.12e+02	6.44e+02
cyl. length	l_c	cm	17.35	10.41	7.44	5.78	4.733
cyl. radius	r_c	cm	1.0	1.0	1.0	1.0	1.000
gap height	g_c	mm	1.305	2.021	0.709	1.171	1.750
wall thickness	w_c	mm	10.0	5.0	2.0	2.0	2.0
capacitance	C_c	pF	27.076	5.245	1.859	0.874	0.479
inductance	L_c	nF	1670	3.10	4.47	5.74	7.02
skin depth	δ_s	μm	2.384	1.847	1.561	1.377	1.245
effective resistance	R_c	m Ω	2.55	5.49	9.09	13.26	17.91
cav. trans. time	Δ_t	ns	0.668	0.401	0.286	0.223	0.182
entry cycle adv.	$\Delta_t f_c l_b / l_c$		0.041	0.068	0.096	0.123	0.150
single pass energy	$U_{1,max}$	J	1.9e-37	1.0e-36	2.8e-36	6.0e-36	1.1e-35
sat. cap. volt.	$V_{C,sat}$	V	1.0e-10	5.6e-10	1.4e-09	2.6e-09	4.3e-09
sat. cap. charge	$Q_{C,sat}$	C	2.8e-21	2.9e-21	2.6e-21	2.3e-21	2.1e-21
sat. ind. curr.	$I_{L,sat}$	A	1.3e-11	2.3e-11	2.9e-11	3.2e-11	3.6e-11
signal power	P_{sig}	W	4.39e-22	4.03e-21	5.11e-20	1.09e-19	2.0e-19
therm. noise floor @1s	P_{noise}	W	4.05e-21	4.05e-21	5.72e-21	5.72e-21	5.72e-21
signal/noise at 1 s	$\log_{10}(P_{sig}/P_{noise})$	db	-9.65	-0.01	9.51	12.78	15.40
signal/noise at 100 s	" + 20	db	10.35	19.99	29.51	32.78	35.40

Table 2: Parameters for split-cylinder polarimeter with candidate resonant frequencies less than 3 GHz (i.e. odd harmonic numbers $h_c \leq 11$), but with $h_c = 1$ (with sapphire dielectric) excluded as being inconveniently long. The cylinder length l_c is fixed by the cavity transit time condition, and the cylinder radius $r_c = 1$ cm is arbitrarily held constant. The capacitance-determining parameters g_c and w_c have been varied from the $h_c = 11$ case analysed so far, and are not necessarily at all optimal, especially at the low frequency $h_c = 3$ extreme. The capacitance C_c itself should be roughly valid though. The bottom two rows neglect all noise sources other than thermal, as well as possible phase noise effects. With intentional phase modulation, the entries in these rows can be less optimistic than shown, but not more.

Eq. (26), excitation. Dividing these equations produces

$$\frac{W_1^{m.a.}}{U_{pol.}} \mathcal{S}^{m.a.} \mathcal{S}^{pol.} = \frac{\left(4.5 \times 10^{-20} \text{ J/m} \right) \left(|\rho| \Delta\theta_{\perp} \frac{\Delta I_{ave}}{I_{ave}} \right)}{\left(M_r^2 \times 1.0899 \times 10^{-35} \text{ J} \right)} \mathcal{S}^{m.a.} \mathcal{S}^{pol.} \approx 10^{10} \left(|\rho| \Delta\theta_{\perp} \frac{\Delta I_{ave}}{I_{ave}} \right) \mathcal{S}^{m.a.} \mathcal{S}^{pol.} \quad (29)$$

where M_r^2 resonant enhancement factors are given in Table 2, and have all been roughly approximated by 5×10^5 in this equation. The final factor $\mathcal{S}^{m.a.} \mathcal{S}^{pol.}$ has been included to incorporate background rejection factors enabled by differential modulation of one or the other of the beam polarization and the beam angle of incidence on the polarimeter.

The huge 10^{10} numerical factor, can be understood as coming, primarily, from the ratio of fundamental constants given in Eq. (1). Any accurate measurement of beam polarization has to rely on this huge factor being overcome. The five factors available to do this appear in the final expression in Eq. (29).

The first of these factors refers to beam centroid offset (measured in meters) at the polarimeter and the second to beam centroid angular offset at the resonator. The third factor quantifies the extent to which the A and B beams are exactly the same, except for opposite polarization. In all three of these cases background rejection comes in two steps, the first of which is precision alignment and the

second is operational improvement. It is pretty clear that operational improvement will be needed, but careful initial alignment will help to make the operational refinement more sensitive.

Estimated values for initial set-up specifications, and expected operational improvement factors are given in Table 3. The initial set-up specifications are quite conservative, but there may not be much point in obsessive improvement of initial positioning and alignment since, without operational improvement, the setup conditions, however careful, are unlikely to provide sufficient background suppression.

Accepting the analysis implied by Table 3, along with the thermal noise reduction described earlier, there is ample background background rejection to provide an accurate polarization measurement in minute-long runs.

Though the table entries are fairly conservative, and the predicted background rejection unnecessarily high, the following reservation has to be made. It is not obvious that the factors given in the table are sufficiently independent of each other, or can all be implemented simultaneously. This analysis has therefore only shown resonant polarimetry to be promising and worth pursuing. Actual success will depend on experimental verification.

misalignment	misalignment factor formula	installation specification	operational improvement factor	background reduction factor
beam position	$\sqrt{\sigma_x^2 + \sigma_y^2}$	< 0.001 m	$/10^2$	$1e-5$
beam slope	$\sqrt{\sigma_{x'}^2 + \sigma_{y'}^2}$	< 0.001	$/10$	$1e-4$
beam imbalance	$\Delta I_{ave}/I_{ave}$	< 0.01	$/10$	$1e-3$
polarization modulation	$\mathcal{S}^{pol.}$		$/10$	$1e-1$
slope modulation	$\mathcal{S}^{m.a.}$		$/10$	$1e-1$
background fraction	$10^{10} \mathcal{S}^{m.a.} \mathcal{S}^{pol.} W_I^{m.a.}/U^{pol.}$			$1e-4$

Table 3: Accumulated background suppression factors from Eq. (29). $|\rho| = \sqrt{\sigma_x^2 + \sigma_y^2}$; $\Delta\theta_{\perp} = \sqrt{\sigma_{x'}^2 + \sigma_{y'}^2}$. Beam position and slope operational improvement factors rely on beam steering of unpolarized beam to null the responses. Beam imbalance improvement relies on downstream nulling of A and B beam currents and on nulling the sub-harmonic leakage in an external beam charge detector. Modulation background suppression factors are guesses that are pessimistic in magnitude, but optimist in the sense that simultaneous modulation of two beam parameters may be impractical. For successful polarization the accumulated factor has to overcome the 10^{10} background advantage factor in the Eq. (29) coefficient that is included in the bottom line.

11 Recapitulation and conclusions

For resonator parameters shown in Table 1, the maximum charge $Q_1^{\text{sat.}}$ residing on the resonator capacitor, after a bunch has made a single passage, has been given in Eq. (12). Figure 9 shows the capacitor charge building up constructively over a few early excitation pulses. The synchronism has been arranged so that every entrance and exit Lenz law excitation is constructive, and the V_C excitation accumulates up to the steady state shown in Figure 10,

Multiplying the V_C response shown in this figure by 10 (to correct for the actual circuit resistance r_c having been artificially increased by a factor of 10 to reduce the computation time) the capacitor build-up factor when steady state has been reached is approximately 600. (As expected) this is less than the resonator Q value of 6760 by a factor more or less equal to the $h_c = 11$ resonator harmonic number. (We refer to Q/h_c as “effective quality factor”, to make allowance for the fact that the quality factor measures damping once per cycle, while the excitation occurs only once per h_c cycles.) Incorporating this factor, the capacitor voltage settles to a steady state value of $Q_{\text{eff.}} Q_1^{\text{sat.}}$, and the saturation level capacitor voltage is $V_C^{\text{sat.}} = (Q/h_c) Q_1^{\text{sat.}}/C_c$. Accepting the multi-element polarimeter circuitry described in Section 7 as valid in every respect, the voltage at the receiver will be increased by a factor equal to the number of pick-ups, which we have here taken to be $N_d = 8$. The saturation level excitation voltage will then be

$$V_C^{\text{rcvr.}} = \frac{N_d(Q/h_c) Q_1^{\text{sat.}}}{C_c} = 3.238 \times 10^{-8} \text{ V.} \quad (30)$$

From Table 2, for a data collection interval of one second, this signal can be expected to be 15.4 db above the thermal noise floor. At that level, even if background and foreground signals are comparable in magnitude, subsequent operational tuning mechanisms have been described for the further isolation of the foreground magnetization signal. This is the basis for our confidence that resonant polarimetry for electrons will be practical.

The same table shows that, as well as for $h_c = 11$, polarimeter performance could also be satisfactory at frequencies corresponding to harmonic numbers $h_c = 7$ or $h_c = 9$. The choice among these three candidates will be governed by construction and data processing considerations.

In conclusion, I correlate the present proposal with similar previous proposals. There has been a considerable history, and much controversy concerning the feasibility of resonant polarimetry. This form of polarimetry was first proposed by Derbenev[9] in 1993, and revived by Conte and others[10] in 2000. At that time a test was proposed at the MIT Bates Lab[11].

Analysis using careful relativistic transformation to a reference frame in which the particle motion is non-relativistic, was performed by Tschalaer at that time, and later, in more detail, in 2008[13], and again in 2015[12]. Tschalaer’s results showed that the previous proposals had overestimated the resonant excitation by (at least) one power of the (large) relativistic factor γ . Perhaps for this reason, the test proposed at the MIT Bates lab was not seriously pursued, or at least not reported in detail.

To avoid serious conceptual difficulty concerning Lorentz transformation, the present proposal has made no explicit use of special relativity. Rather it has taken a purely Maxwellian approach that uses a Faraday’s law formulation in which the resonator excitation is calculated by the straightforward application of Lenz’s law.

For our proposed J-lab test of resonant polarimetry, mindful of Tschalaer’s results, we have chosen $\gamma = 2$, which is the lowest value of γ that can be provided by the CEBAF injector at a convenient location along the beam line. At this γ -value the electron velocity is $0.866c$, which is to say “almost fully relativistic”. It is clear from the Lenz’s law derivation that (except, possibly, for thirteen percent) the same excitation will apply for all larger values of γ . In this respect the result is consistent with Tschalaer—certainly it does not contradict his claim that there is no effect that increases proportional to γ .

As far as I am concerned this lays to rest a decades old controversy concerning the γ -dependence of cavity excitation by a passing bunch of polarized particles. Like Tschalaer, this paper has shown that,

once the particles have become fully relativistic, there is no further γ -dependence of the resonator excitation.

But this is not the main content of the present paper. Rather, what has been demonstrated is the design of a non-destructive resonant electron polarimeter capable of measuring the polarization state of a relativistic electron beam non-destructively, and with high accuracy. To be fully persuasive, however, actual experimental verification is necessary. Such a test at Jefferson lab is under active planning.

This paper has profited greatly from regular conferences with my colleagues planning for a Jefferson Lab test: Joe Grames, Alicia Hofler, Reza Kazimi, Matt Poelker, and Riad Suleiman, and, especially concerning polarimeter design, Brock Roberts. I have also profited from numerous theoretical discussions with Saul Teukolsky, Eanna Flanagan, Bob Meller, Alex Chao, Yunhai Cai, Gennady Stupakov, and Wolfgang Hillert.

References

- [1] W. Hardy and L. Whitehead, *Split-ring resonator for use in magnetic resonance from 200-2000 MHz*, Review of Scientific Instruments, **52** (2) 213, 1981
- [2] B. R. Johnson, *Nuclear Spin Waves in Spin-Polarized Hydrogen*, Cornell Ph.D. thesis, 1984
- [3] Storage Ring EDM Collaboration, *A Proposal to Measure the Proton Electric Dipole Moment with 10^{-29} e-cm Sensitivity*, October, 2011
- [4] J. Jackson, *Classical Electrodynamics*, 3rd edition, John Wiley, 1998
- [5] W. Smythe, *Static and dynamic electricity*, 2nd edition, McGraw Hill, 1950
- [6] V. Kumar, *Understanding the focusing of charged particle beams in a solenoid magnetic field*, Am. J. Phys. **77** (8) 2009
- [7] C. Montgomery, R. Dicke, and E. Purcell, *Principles of Microwave Circuits*, McGraw-Hill, 1948
- [8] N. Mott and H. Massey, *The Theory of Atomic Collisions*, 3rd Edition, p. 229, 1965
- [9] Ya. S. Derbenev, *RF-resonance beam polarimeter, Part I. Fundamental concepts*, Nuclear Instruments and Methods in Physics Research A 336, 12-15, 1993
- [10] M. Conte, et al., *The Stern-Gerlach interaction between a traveling particle and a time varying magnetic field*, arXiv:physics/0003069v1 [physics.acc-ph], 2000
- [11] P. Cameron, et al., *An RF Resonance Polarimeter Phase I Proof of Principle Experiment*, RHIC/AP/126
- [12] C. Tschalaer, *The Relativistic Stern-Gerlach Force*, arXiv/papers/0802/0802:0154.pdf, 2008
- [13] C. Tschalaer, *Lorentz Transform of an Arbitrary Force Field on a Particle in its Rest Frame using the Hamilton-Lagrangian Formalism*, BIR#15-01, Bates Lab Report, 2015